Ceramics International 47 (2021) 26335–26349

Contents lists available at ScienceDirect

Ceramics International

journal homepage: www.elsevier.com/locate/ceramint

Study on recycled Er-incorporated waste CRT glasses for photon and neutron shielding

R. Kurtuluş [a], T. Kavas [a], O. Agar [b], M.F. Turhan [c], M.R. Kaçal [d], I. Dursun [e,f], F. Akman [f,g,*]

[a] Afyon Kocatepe University, Faculty of Engineering, Department of Materials Science and Engineering, 03200, Afyonkarahisar, Turkey
[b] Karamanoğlu Mehmetbey University, Department of Medical Imaging Techniques, 70100, Karaman, Turkey
[c] Afyonkarahisar Health Sciences University, Atatürk Vocational School of Health Service, Department of Medical Imaging Techniques, 03200, Afyonkarahisar, Turkey
[d] Giresun University, Arts and Sciences Faculty, Department of Physics, 28100, Giresun, Turkey
[e] Bingöl University, Unit of Pilot University Coordination Center, 12000, Bingöl, Turkey
[f] Bingöl University, Central Laboratory Application and Research Center, 12000, Bingöl, Turkey
[g] Bingöl University, Vocational School of Social Sciences, Department of Property Protection and Security, Program of Occupational Health and Safety, 12000, Bingöl, Turkey

ARTICLE INFO

Keywords:
CRT glasses
Er_2O_3
Radiation shielding
HPGe detector
Waste valorization

ABSTRACT

The present study is extremely associated with the evaluation of cathode ray tube (CRT) waste which is a growing hazardous waste management and disposal issue. The Er-added recycled glasses derived from CRT have been successfully fabricated as a component for Na_2O–Al_2O_3–SiO_2–K_2O–CaO–SrO–BaO–PbO–Fe_2O_3–TiO_2–Er_2O_3 glass systems. The waste cathode ray tube panel glass (WPG) series were obtained by inserting the Er_2O_3 in substitution for CRT in the amounts of 0, 1, 3 and 5 mol%. The synthesized WPG series were then subjected to numerous characterization analysis. One can firmly report that the insertion ratio from 0 to 5 mol% in Er_2O_3 increased the glass density from 2.9216 to 2.9763 g/cm^3. Further, there exists no crystalline formation with the addition of Er_2O_3, instead, an amorphous nature in all WPG series emerges. Microstructural images captured by the SEM technique also confirm the non-crystallinity of the fabricated samples. Energy dispersive spectroscopy (EDS) in SEM, besides, paved the way for revealing the elemental mapping of the WPG series. From the perspective of radiation shielding competencies, nuclear shielding features have been evaluated in terms of μ_m and related attenuation parameters at several photon energies of 276.4–1332.5 keV by utilizing narrow beam transmission methods. The experimental data have been also confirmed to those of theoretical results by WinXCom software. The HVL results revealed superior photon radiation shielding performances for recycled WPG glasses in comparison to various concretes. In addition, exposure buildup factor (EBF) values estimated utilizing the G-P fitting approach would be useful to design or develop the synthesized glass systems for shielding applications. Furthermore, the macroscopic effective removal cross-sections for fast neutron (Σ_R) have been estimated. In conclusion, the findings clearly demonstrated that Er-incorporated CRT glasses can effectively be implemented in radiation shielding applications instead of Pb having toxic effects.

1. Introduction

With the rapid development of industrial technology, there has been a great technological revolution. Although living standards are improving, the amount of waste is rapidly increasing worldwide. Therefore, treatment and management of industrial waste have become essential for protecting the environment and natural resources [1,2]. In the last few decades, thinner and lighter versions such as liquid crystal displays (LCD), plasma display panels (PDP) and light emitting diode (LED) are continuously preferred instead of the cathode ray tubes (CRTs) which are an essential part of computer and television display monitors [3,4]. Thus, it can be easily predicted that a huge number of waste CRTs are among different types of industrial waste which need to be disposed urgently according to statistical data reported in many studies [5–8].

One of the encouraging and effective techniques to decrease environmental influence of waste CRT glasses is to re-use by adding into a raw material for different purposes. Therefore, it offers various advantages such as eliminating the costs of disposing, reducing soil and air

* Corresponding author. Bingöl University, Central Laboratory Application and Research Center, 12000, Bingöl, Turkey.
E-mail address: fakman@bingol.edu.tr (F. Akman).

https://doi.org/10.1016/j.ceramint.2021.06.044
Received 1 January 2021; Received in revised form 8 May 2021; Accepted 4 June 2021
Available online 8 June 2021

Fig. 1. The waste CRT glass used in this work.

Table 1
The related codes, chemical compositions (wt%) and densities (g/cm^3) of glass series.

Code	Na_2O	K_2O	Al_2O_3	TiO_2	SiO_2	CaO	BaO	SrO	PbO	Fe_2O_3	Er_2O_3	ρ
WPG0	5.190	9.290	4.640	0.390	60.560	2.090	7.490	9.980	0.170	0.200	0.000	2.9216
WPG1	5.138	9.197	4.594	0.386	59.954	2.069	7.415	9.880	0.168	0.198	1.000	2.9322
WPG3	5.034	9.011	4.501	0.378	58.743	2.027	7.265	9.681	0.165	0.194	3.000	2.9539
WPG5	4.931	8.826	4.408	0.371	57.532	1.986	7.116	9.481	0.162	0.190	5.000	2.9763

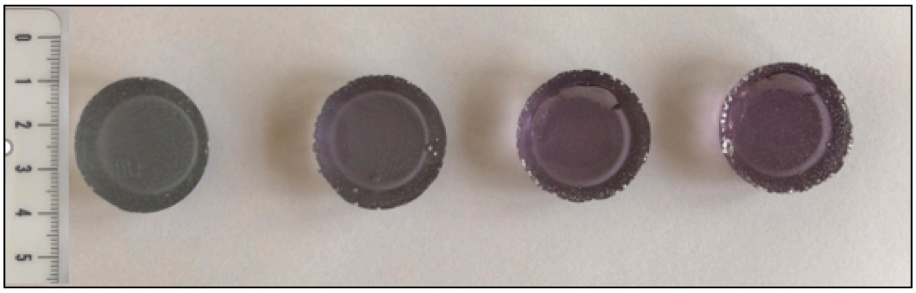

Fig. 2. The photo of the fabricated WPG glass series (from left to right: 0, 1, 3 and 5 mol% Er_2O_3 addition).

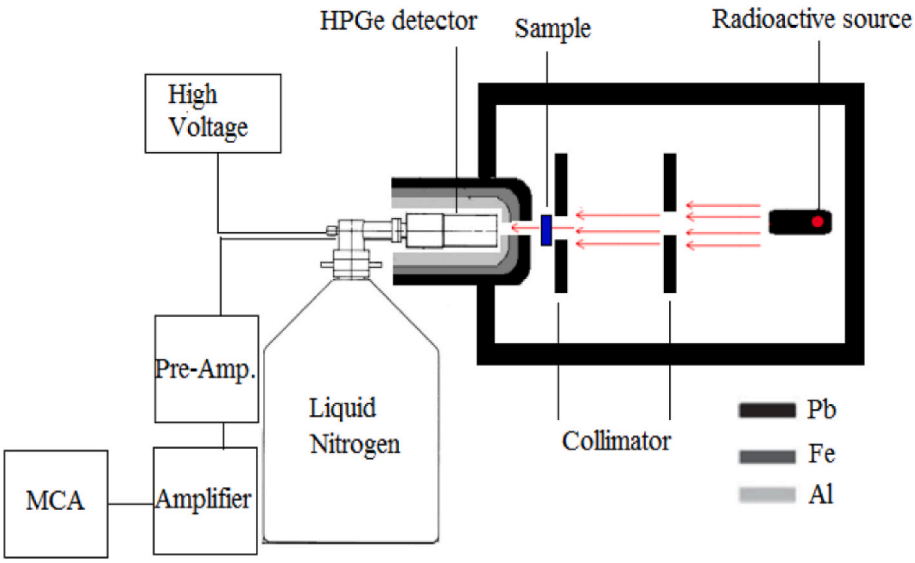

Fig. 3. Narrow beam transmission geometry of the experimental system, where the distances between the gamma ray source and the sample, and to increase the detection efficiency due to detector dead time, the window of the HPGe detector and the sample are 14 cm and 1 cm, respectively.

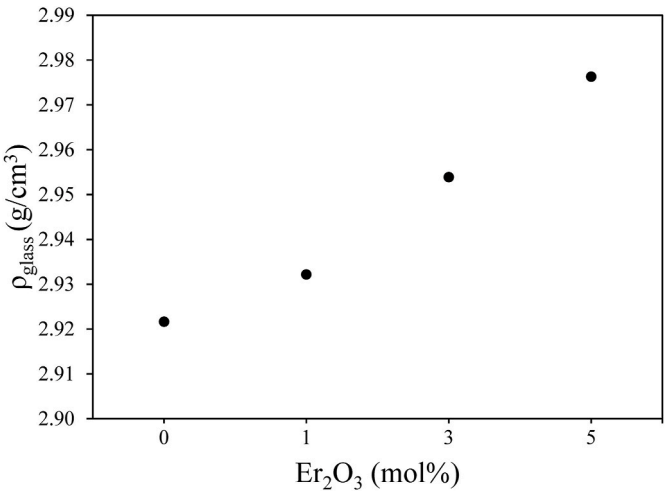

Fig. 4. Alteration of glass density (ρ_{glass}) with respect to Er_2O_3 contribution in mol%.

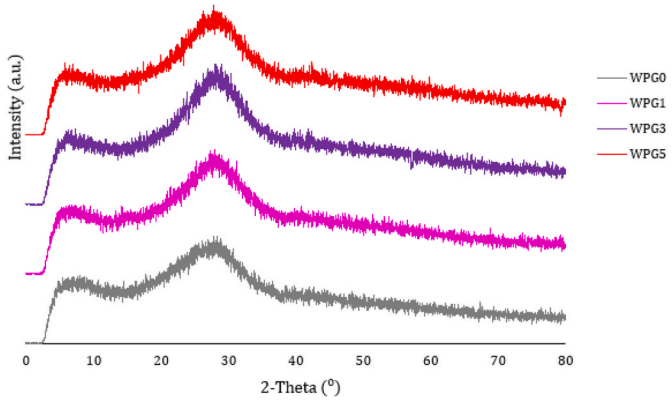

Fig. 5. XRD patterns of WPG samples.

pollution issues, conservation of natural resources [9]. There have been a number of previous studies on surveying the recycled possibilities in two important routes as closed-loop recycling (glass-to-glass, old CRT glass to new CRT glass) and open-loop recycling (glass-to-products) [10–13]. Recycled CRT glasses are quite remarkable as a significant source in preparation as alternative nuclear shielding glass material due their unique features with excellent corrosion resistance, transparency and high strength [14,15]. In addition to this, developing the chemical durability of CRT glasses can be provided by adding rare earth (RE) based oxide such as Er_2O_3 with both its lower oxidizing in air and stability [16].

As well known, various chemical compounds doped glasses such as borate [17–20], silicate [21–23], germenate [24,25] and phosphate [26–31] have been evaluated in terms of nuclear radiation shields. Although various researchers have studied to investigate the feasible study of waste CRTs in the fabrication of glasses [32–34], a detailed comparison of the effect on X- and gamma rays shielding performance, especially neutron radiation is still relatively limited. In order to maximize the recycling of this industrial waste material, this research aims to present a detailed investigation on physical, structural, photon and neutron radiation shielding characteristics of some Er-doped recycled CRT glasses. The energy absorption build-up factor (EABF) and exposure build-up factor (EBF) have been calculated utilizing G-P fitting method for incident photon energy of 0.015–15 MeV.

2. Materials and methods

2.1. Glass synthesis

In order to fabricate radiation shielding glass systems consisted of waste cathode ray tube (CRT) panel (WPG) containing various amounts of Er_2O_3, five main steps have been followed: *waste supply, glass powder obtainment, batch preparation, melting, and annealing*. Each step is thoroughly explained under the below-given subtitles.

i. Waste procurement

Initially, a waste CRT monitor was supplied from the electronic disposal storage area located at Afyon Kocatepe University. Every single component of the CRT monitor was disassembled. Then, the WPG series were obtained utilizing waste glasses part in CRT. Accordingly, the mentioned operations were detailly displayed in Fig. 1. After the WPG was taken out of the case, it was cleaned through water following by drying in an oven at 110 °C for 2 h.

ii. Glass powder obtainment

In this step, the WPG powders were obtained by following three processes. First, the WPG was broken using a 5 kg-steel hammer after wrapping out with a paper towel to prevent any iron oxide (Fe_2O_3) contamination. The fractured glass pieces were then subjected to grinding operation with the use of a rotary mill composed of a porcelain jar including alumina balls inside. The grinding process was continued until particle sizes lowering than 250 μm are achieved. The chemical composition of WPG powders, $5.19Na_2O$-$4.64Al_2O_3$-$60.56SiO_2$-$9.29K_2O$-$2.09CaO$-$9.98SrO$-$7.49BaO$-$0.17PbO$-$0.20Fe_2O_3$-$0.39TiO_2$ in wt %, was determined via X-rays fluorescence (XRF) measurement technique (Rigaku ZSX Primus). In addition to the WPG powder obtainment, erbium oxide (Er_2O_3) as the reinforcing substance was procured from Sigma Aldrich with a purity of 99.99%.

iii. Batch preparation

The prepared starting materials paved the way for glass batch design. To understand the effect of Er_2O_3 on raw glass, different amounts as 1, 3, and 5 wt% was added in substitution for WPG. Table 1 summarizes the glass chemical compositions, densities and related codes of the fabricated glasses. Following glass compositions design, the relevant amounts for each starting material were weighed via an analytical scale having ±0.0001 g tolerance. The weighed batch series were then mixed in a rotary mill at 250 rpm for 1 h to obtain a homogeneous mixture. At eventual, each mixture of glass series was made ready for the melting step.

iv. Melting

The melting process was performed by utilizing an elevator furnace (MSE_1600_18) capable of reaching up to 1600 °C. In this process, the mixtures were placed into the Au–Pt crucible followed by melting at 1300 °C for 2 h. After melting completed, the Au–Pt crucible was taken out from the furnace to the ambient temperature. Five mins were allowed to stand in this situation, and finally, the glass specimens were removed from the crucible without any cracking.

v. Annealing

In order to relieve the residual stress inside the glass samples after the melting step, the annealing process was carried out with the temperature profile decreasing from 550 °C to room temperature with the steps of 10 °C/min. After the annealing process completed, the photos of the fabricated glass series were captured by using a mobile phone

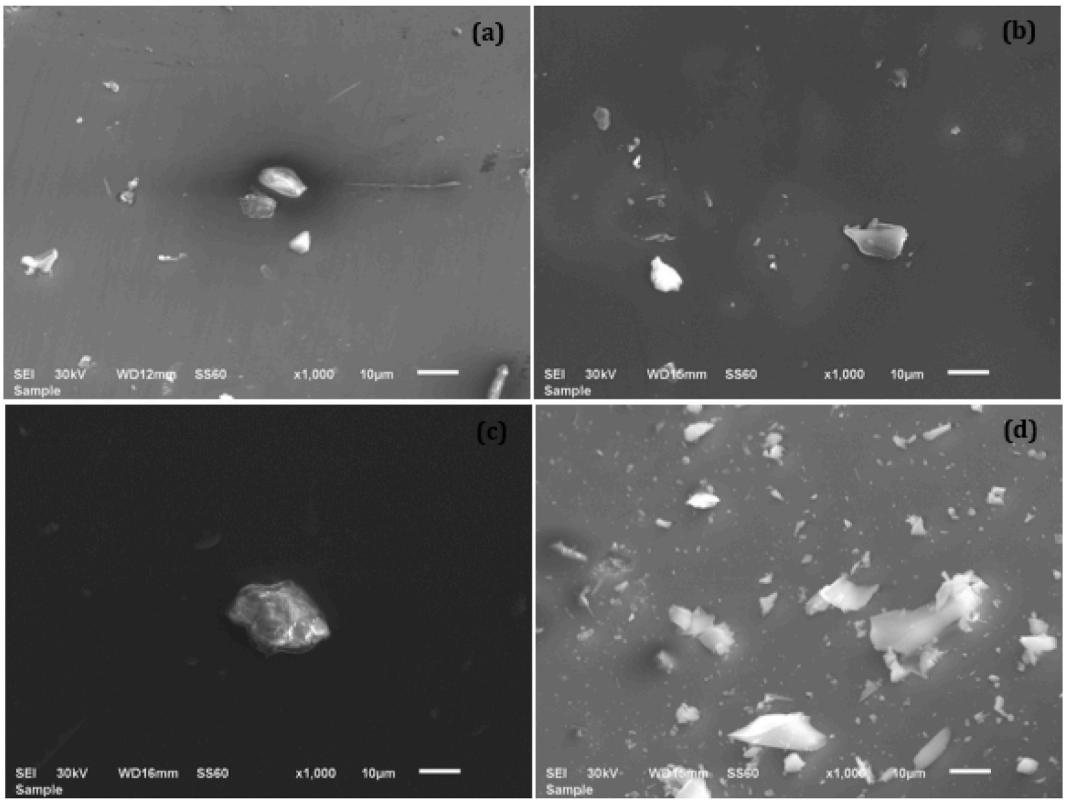

Fig. 6. SEM images of the fabricated WPG series at 1.000X magnification (from a to d: WPG0, WPG1, WPG3, and WPG5).

camera with a 12 MP and shown in Fig. 2.

2.2. Glass characterizations

For understanding the effect of Er_2O_3 in the WPG system on glass density (ρ_{glass}), the Archimedes principle given in Eq. (1) was employed. Here, m_{air} and m_{liquid} indicate the weight of glass in air and in demineralized water, respectively.

$$\rho_{glass} = \frac{m_{air}}{m_{air} - m_{liquid}} \tag{1}$$

X-ray diffraction (XRD) measurement was performed via Rigaku device by using CuK_α at 40 kV and 30 mA with the scanning step of 0.02 between 0 and 80° in order to observe the glass structure.

The morphology of the fabricated glass series was observed via scanning electron microscopy (SEM) device (JEOL-JSM6510) utilized at 30.0 kV accelaration voltage. Further, elemental mapping was done via EDX/SEM technique to reveal the elemental contents of the glass series.

2.3. Gamma shielding methodology

The investigation on gamma shielding performance of the prepared materials was performed experimentally at laboratory frame and theoretically with a computer-based program. Both theoretical and experimental details have been explained in following subheads.

2.3.1. Theoretical background

Linear attenuation coefficient, μ, is related to measure of the reduction in gamma ray intensities moving through any absorber and can be calculated through Beer-Lambert relation, where I_0 and I photon intensities denote "un-attenuated" and "attenuated" measurements, respectively [35]:

$$\mu = -\frac{\ln \frac{I}{I_0}}{x} \tag{2}$$

Here, x is thickness of the sample.

The precision of the designed layout and photon attenuation of the glass can be verified with using well-known mixture rule [36]:

$$\mu_m = \frac{\mu}{\rho} = \sum w_i \left(\frac{\mu}{\rho}\right)_i \tag{3}$$

where μ_m and ρ represent the mass attenuation coefficient ($cm^2\ g^{-1}$) and the density ($g\ cm^{-3}$) of the absorber.

Another parameters to be carefully investigated before the application of any attenuator is effective atomic number (Z_{eff}) and effective electron density (N_E) can be derived [37,38]:

$$Z_{eff} = \frac{\sum_i f_i A_i (\mu/\rho)_i}{\sum_i f_i \left(\frac{A_i}{Z_i}\right)(\mu/\rho)_i} \tag{4}$$

$$N_E = \frac{Z_{eff}}{A_{tot}}(N_A n_{tot}) \tag{5}$$

where A_i, f_i, Z_i, N_A, n_{tot} and A_{tot} stand for the atomic weight, the fraction by mole of each constituent element of the glass, the atomic number, Avogadro number, total element number and total atomic weight in the glass, respectively.

Some useful shielding parameters such as HVL, TVL and MFP which represent the needed thickness of the sample attenuating original gamma ray intensity to 50%, 10% and 36.8%, respectively. In order to reveal the mathematical statements of HVL, TVL and MFP parameters, Beer-Lambert rules can be easily altered to ln2/μ, ln10/μ and 1/μ equations, respectively [39,40].

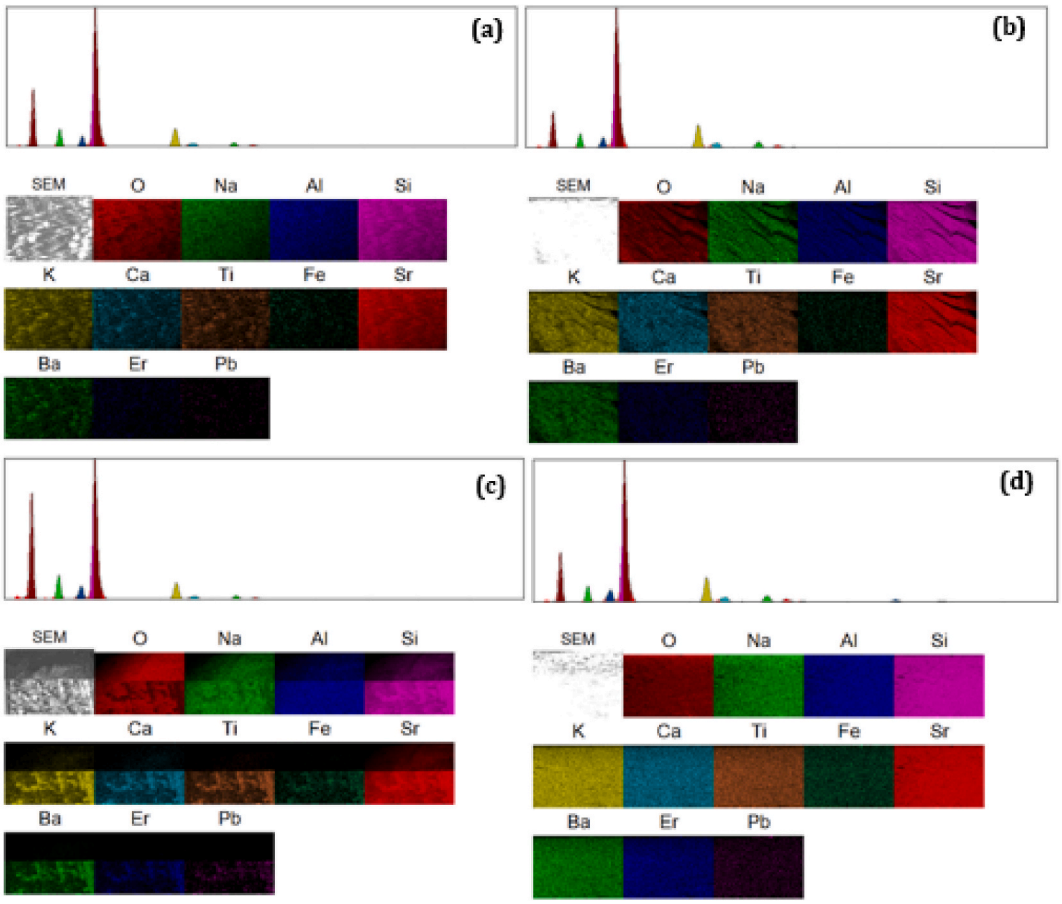

Fig. 7. Elemental mapping of the synthesized glass series via EDX/SEM technique (from a to d: WPG0, WPG1, WPG3, and WPG5).

Table 2
Experimental and theoretical mass attenuation coefficient values for prepared glass samples and R.D. values.

Energy (keV)	Mass attenuation coefficients (cm^2/g)											
	WPG0			WPG1			WPG3			WPG5		
	Exp.	XCOM	R.D.	Exp.	XCOM	R.D.	Exp.	XCOM	R.D.	Exp.	XCOM	R.D.
276.4	0.1239 ± 0.0058	0.1205	2.75	0.1244 ± 0.0058	0.1223	1.72	0.1312 ± 0.0049	0.1257	4.43	0.1232 ± 0.0061	0.1291	4.63
302.9	0.1106 ± 0.0042	0.1140	3.01	0.1125 ± 0.0041	0.1154	2.49	0.1233 ± 0.0062	0.1180	4.47	0.1267 ± 0.0066	0.1207	4.98
356.0	0.1006 ± 0.0034	0.1042	3.43	0.1033 ± 0.0033	0.1051	1.68	0.1101 ± 0.0034	0.1067	3.22	0.1079 ± 0.0036	0.1084	0.45
383.9	0.1026 ± 0.0047	0.1001	2.43	0.1068 ± 0.0053	0.1008	5.94	0.1075 ± 0.0066	0.1021	5.21	0.1043 ± 0.0051	0.1035	0.74
511.0	0.0878 ± 0.0023	0.0868	1.13	0.0918 ± 0.0036	0.0871	5.47	0.0874 ± 0.0035	0.0876	0.31	0.0899 ± 0.0033	0.0882	1.89
661.7	0.0773 ± 0.0032	0.0766	0.95	0.0804 ± 0.0031	0.0767	4.89	0.0818 ± 0.0033	0.0769	6.38	0.0789 ± 0.0033	0.0772	2.19
1173.2	0.0538 ± 0.0024	0.0576	6.61	0.0603 ± 0.0024	0.0576	4.82	0.0584 ± 0.0031	0.0575	1.49	0.0598 ± 0.0030	0.0575	3.86
1274.5	0.0520 ± 0.0015	0.0552	5.73	0.0569 ± 0.0015	0.0552	3.17	0.0530 ± 0.0025	0.0551	3.78	0.0520 ± 0.0025	0.0551	5.65
1332.5	0.0547 ± 0.0029	0.0539	1.38	0.0551 ± 0.0037	0.0539	2.17	0.0569 ± 0.0030	0.0539	5.65	0.0557 ± 0.0029	0.0538	3.46

2.3.2. *Experimental measurements*

The experimental layout displayed in Fig. 3 was firstly set for the measurements. The narrow beam transmission geometry was involved basically gamma spectrometry system consisted of high voltage source, preamplifier, amplifier, multi-channel analyzer (MCA) and basic HPGe detector as well as several radioactive point sources [41,42]. Moreover, Pb collimators with certain thickness were utilized in order to both adjust the beam shape and decrease possible background counts. Thereafter, the gamma ray intensities with the present layout were detected at various photon energies using the point sources of ^{22}Na, ^{60}Co, ^{133}Ba and ^{137}Cs, widely varying from 276.4 to 1332.5 keV [43]. These sources have activities of 413 kBq–473 kBq. The measurements of all the sources were applied for 600 s.

Also, the uncertainties in shielding tests were estimated through the uncertainties in mass per unit area, un-attenuated (I_0) and attenuated photon intensity (I) using the following equation [44]:

$$\Delta\mu_m = \frac{1}{\rho x}\sqrt{\left(\frac{\Delta I}{I}\right)^2 + \left(\frac{\Delta I_0}{I_0}\right)^2 + \ln\left(\frac{\Delta I}{I}\right)^2\left(\frac{\Delta \rho x}{\rho x}\right)^2} \quad (6)$$

2.4. *Calculation procedure of build-up factors and kerma relative to air*

Energy absorption build-up factor (EABF) and exposure build-up factor (EBF) values were determined with the help of the equivalent atomic number (Z_{eq}) and geometric progression (G-P) fitting coefficients for the glass systems. Comprehensive clarification of the geometric progression method used has been already discussed in our previous works [42,45].

Kerma describes the expectation value of the energy transferred to charged particles per unit mass at a certain point in which contain

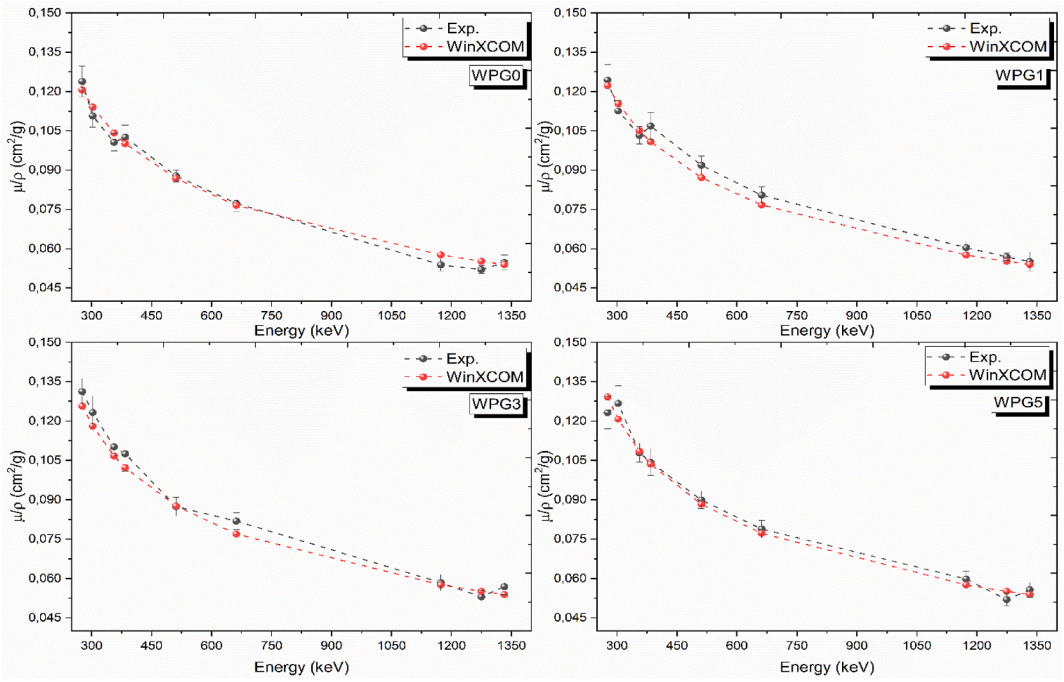

Fig. 8. Graphs of experimental and theoretical mass attenuation coefficient values for prepared glass samples.

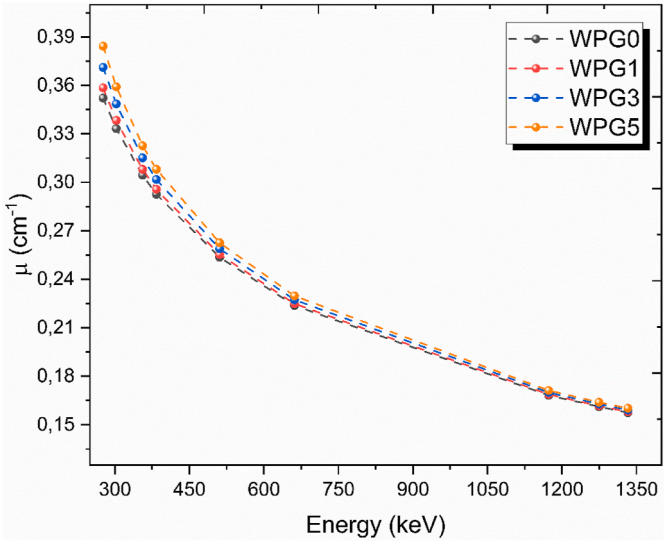

Fig. 9. Linear attenuation coefficient values for prepared glass samples.

radiative-loss energy and excludes energy passed from one charged particle to another [46]. Kerma at an interested point is associated to energy fluence and mass energy absorption coefficient and determined the following equation:

$$K = \Psi\left(\frac{\mu_{en}}{\rho}\right) \tag{7}$$

Here Ψ is the energy fluence, μ_{en} denotes the linear energy transfer coefficient and ρ shows the density of the absorber. Kerma relative to air values of a glass system can be computed using the following equation.

$$\frac{(\mu_{en}/\rho)_{GS}}{(\mu_{en}/\rho)_{Air}} \tag{8}$$

The mass energy absorption coefficient for a glass system is determined with the help of Eq. (9):

$$\left(\frac{\mu_{en}}{\rho}\right)_{GS} = \sum W_i \left(\frac{\mu_{en}}{\rho}\right)_i \tag{9}$$

where the weight fraction is symbolized with W_i and the mass energy absorption coefficient of the *i*th constituent element is symbolized with $(\mu_{en}/\rho)_i$.

2.5. Neutron effective removal cross-section

Macroscopic effective removal cross-section (Σ_R) for the fabricated CRT glasses described as significant neutron shielding parameter can be calculated theoretically [47]:

$$\Sigma_R = \Sigma W_i (\Sigma_{R/\rho})_i \tag{10}$$

3. Results and discussions

3.1. Glass property determinations

The recycled CRT glass series including varying amounts of Er_2O_3 was successfully fabricated. As displayed in Fig. 2, the undoped sample, WPG0, provided a grayish color while Er_2O_3 containing ones, WPG1, WPG3, and WPG5, demonstrated a pinkish color. The pinkish color substantially intensifies with the increasing concentration of Er_2O_3. This situation is somehow plausible due to the inherently coloring effect of Er_2O_3 [48]. Hence, one can deduce that the color of the WPG series shifts to the pinkish side because of the increasing Er_2O_3 insertion ratio.

After discussing the visual aspects of the synthesized glass series, it comes to evaluate one of the most essential parameters, glass density (ρ_{glass}). With the use of ρ_{glass} value in radiation shielding applications, attenuation characteristics can clearly be ascertained. This is because higher ρ_{glass} offers to improve radiation shielding competencies. From this point of view, we performed ρ_{glass} measurements, and Fig. 4 illustrates the ρ_{glass} values with respect to changing Er_2O_3 concentrations. According to the findings, glass density exhibits an increasing trend in virtue of the increasing Er_2O_3 amount. For instance, the WPG0 sample without any contribution yields 2.9216 ± 0.0001 g/cm^3 whereas the

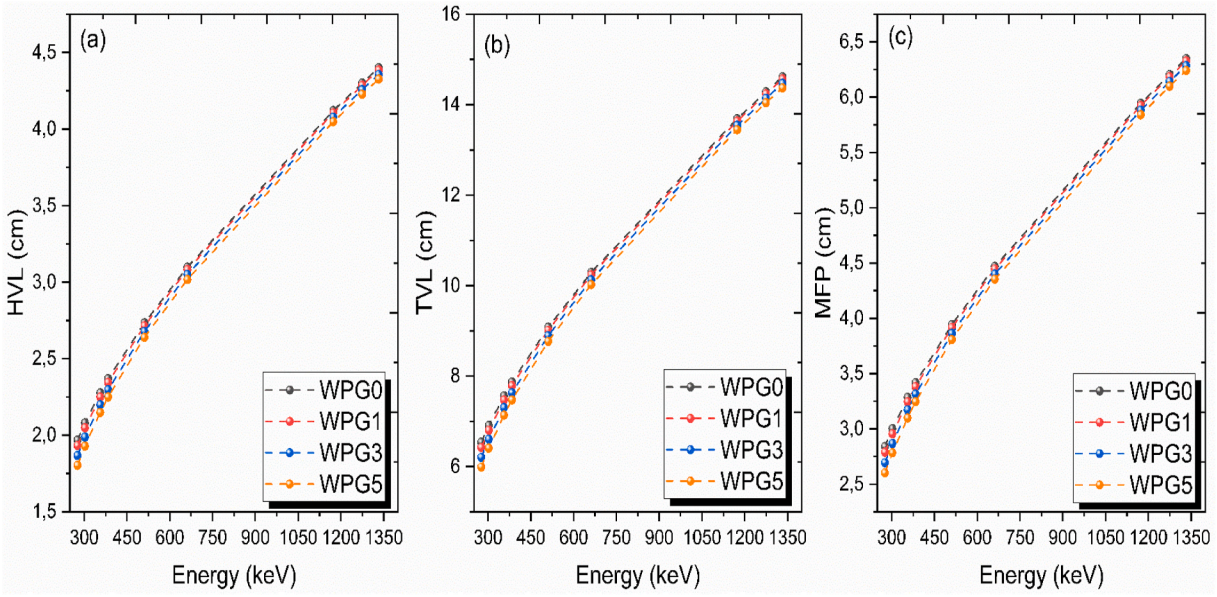

Fig. 10. HVL, TVL and MFP values for prepared glass samples.

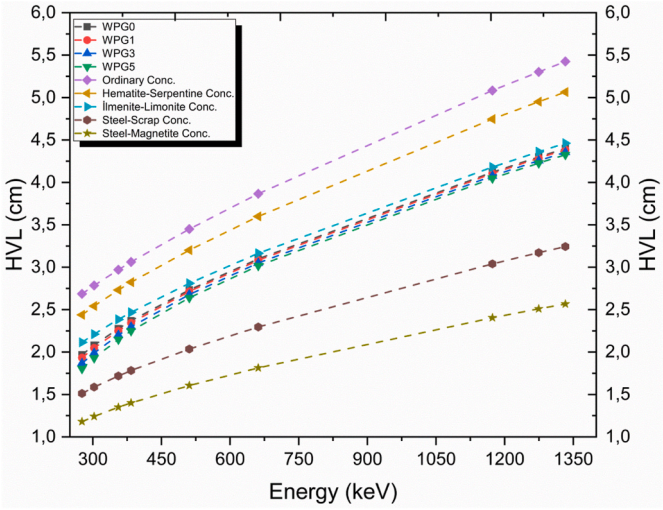

Fig. 11. Comparisons of HVL values for the prepared glass samples with other samples.

WPG5 sample with the highest content presents 2.9763 ± 0.0001 g/cm^3. The increase in ρ_{glass} can be attributed to the higher density value of Er_2O_3 (8.64 g/cm^3) in comparison to the CRT glass (2.9216 g/cm^3). Likewise, some studies [49–51] figured out parallel outcomes with regards to the Er_2O_3 effect on overall ρ_{glass}. In conclusion, the authors report that Er_2O_3 addition can be favorable for enhancing ρ_{glass} which in turn can improve radiation attenuation characteristics.

XRD technique is very effective to understand to observe the crystalline structure of glass substances. Fig. 5 demonstrates the XRD patterns of the fabricated WPG series. At first glance, an amorphous structure for all series is in evidence. This situation can be seen with a hump shape between 15 and 35°. With the insertion ratio of Er_2O_3 from 0 to 5 mol%, no crystalline formation was observed. For that reason, one can conclude that all fabricated WPG series demonstrate an amorphous nature.

Morphology images can provide sufficient knowledge to understand the crystalline nature of the glass systems. Fig. 6 demonstrates the micro-images of the synthesized WPG series captured at 1.000X magnification. One can obviously confirm that all WPG series displayed an amorphous structure with some small crystalline particles. Additionally, no voids or cracks are observable for the fabricated glasses.

Further to the microstructural images, it is essential to observe the elemental existence of the starting oxides in the glass system. For this,

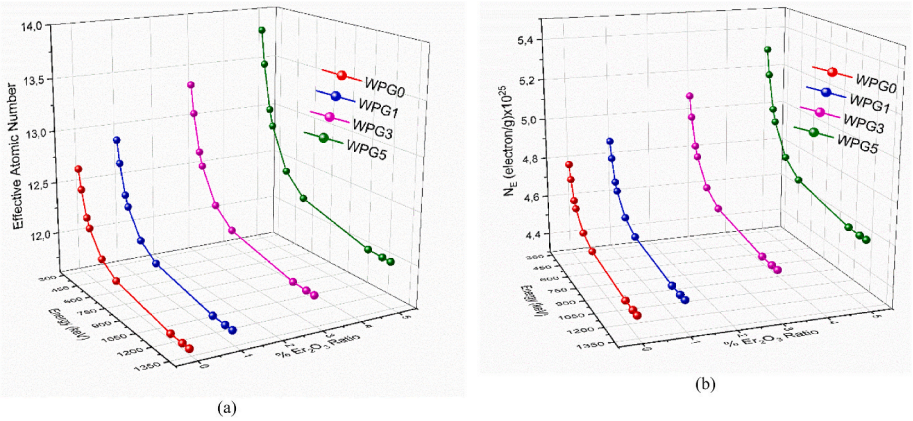

Fig. 12. Effective atomic number and electron density values for prepared glass samples.

Table 3
Experimental and theoretical effective atomic number values for prepared glass samples.

Energy (keV)	Effective Atomic Number							
	WPG0		WPG1		WPG3		WPG5	
	Exp.	Theo.	Exp.	Theo.	Exp.	Theo.	Exp.	Theo.
276.4	12.966 ± 0.610	12.619	13.073 ± 0.611	12.852	13.899 ± 0.520	13.309	13.148 ± 0.654	13.786
302.9	12.055 ± 0.460	12.430	12.319 ± 0.450	12.633	13.615 ± 0.680	13.033	14.121 ± 0.740	13.451
356.0	11.764 ± 0.397	12.181	12.137 ± 0.392	12.345	13.075 ± 0.406	12.667	12.946 ± 0.432	13.005
383.9	12.387 ± 0.563	12.093	12.970 ± 0.641	12.243	13.190 ± 0.813	12.538	12.941 ± 0.628	12.847
511.0	12.004 ± 0.313	11.870	12.638 ± 0.492	11.983	12.169 ± 0.491	12.206	12.675 ± 0.468	12.440
661.7	11.873 ± 0.491	11.761	12.436 ± 0.479	11.857	12.812 ± 0.512	12.044	12.509 ± 0.521	12.241
1173.2	10.885 ± 0.476	11.656	12.298 ± 0.485	11.733	12.063 ± 0.632	11.885	12.511 ± 0.637	12.046
1274.5	10.984 ± 0.310	11.652	12.100 ± 0.322	11.728	11.429 ± 0.538	11.879	11.357 ± 0.540	12.037
1332.5	11.812 ± 0.617	11.651	11.982 ± 0.796	11.727	12.548 ± 0.661	11.877	12.452 ± 0.644	12.035

Table 4
Equivalent atomic numbers of the WPGX (X = 0, 1, 3, 5) glass series for the energy range from 0.015 to 15 MeV.

Energy (MeV)	WPG0	WPG1	WPG3	WPG5
0.015	14.971	15.300	15.890	16.471
0.02	18.377	18.594	18.996	19.415
0.03	18.927	19.153	19.580	19.994
0.04	23.646	23.771	24.009	24.257
0.05	23.159	23.284	24.522	24.761
0.06	23.547	25.430	26.979	28.425
0.08	25.119	26.056	27.704	29.212
0.1	25.757	26.719	28.399	29.924
0.15	26.443	27.468	29.245	30.850
0.2	26.867	27.935	29.759	31.405
0.3	27.369	28.485	30.389	32.094
0.4	27.669	28.822	30.762	32.491
0.5	27.862	29.035	31.007	32.750
0.6	27.990	29.163	31.158	32.922
0.8	28.108	29.299	31.312	33.095
1	28.140	29.336	31.356	33.147
1.5	24.153	25.374	27.496	29.422
2	19.005	19.797	21.322	22.849
3	16.946	17.451	18.426	19.420
4	16.457	16.884	17.709	18.564
5	16.247	16.639	17.403	18.193
6	16.110	16.484	17.210	17.968
8	15.965	16.321	17.010	17.722
10	15.902	16.248	16.918	17.616
15	15.859	16.198	16.858	17.541

the authors implemented an elemental dispersive spectroscopy (EDS) technique via SEM for confirming the oxide contents. In Fig. 7, the elements of the fabricated glass series are in evidence owing to the elemental mapping. In particular, the insertion of Er_2O_3 can easily be seen from the images of a to d. Therefore, we could confirm the existence of the each elemental contents thanks to the EDS analysis.

3.2. Detailed analysis of gamma ray shielding performance

The experimental mass attenuation coefficients (μ_m) of waste recycled CRT glasses included with various amounts of Er_2O_3 as a function of energy are determined by recording the intensity of photons that passes through the samples utilizing a narrow beam transmission (Fig. 3), while the theoretical values were estimated with help of mixture rule based WinXCom program in a wide energy region of 276.4, 302.9, 356.0, 383.9, 661.7, 1173.2, 1274.5 and 1332.5 keV to obtain the accurate data for the radiation shielding parameters. The detailed comparisons of experimental and theoretical values have been summarized in Table 2 and demonstrated in Fig. 8, respectively. Especially, Fig. 8 exhibits easily that the obtained results of different WPG glasses reduce with increasing of photon energy. Furthermore, the experimental uncertainties in μ_m results are found in the range of 2.62–5.30% for WPG0 sample, 2.64–6.72% for WPG1 sample, 3.09–5.27% for WPG3 sample and 3.34–5.21% for WPG5 sample and can be attributed to scattering effects, the counting statistics in intensities of I_0 and I photons (Eq. (2)), and the mass measurement in glass per unit area. These values are evident of how to obtain μ_m and other protection parameters with high accuracy for the examined glasses.

Besides, the relative deviations (RD,%) between the experimental and WinXCom results of μ_m were calculated via the following equation [52]:

$$RD = \left(\frac{\mu_{m,exp.} - \mu_{m,WinXCOM}}{\mu_{m,exp.}}\right) * 100 \quad (11)$$

Table 2 and Fig. 8 contain the consistency of two techniques in the μ_m of the CRT samples. It is evident in Fig. 8 that the obtained μ_m values of the samples under investigation are in good agreement with each other. The obtained RD values given in Table 2 are found in the range of 0.31–6.61% for experimental-WinXCom results. The arisen differences can be based on the mixture rule that ignores the interactions among atoms in a mixture material. Furthermore, these implications on μ_m parameter are supported with the findings reported on $50B_2O_3$+ $20BaCO_3$+ $30Li_2O_3$+ xCo_3O_4: $0 = x \leq 0.5$ mol% by Rammah et al. [53], (30 + x)PbO–10WO_3–10Na_2O–10MgO-(40-x)B_2O_3 glasses by Kumar et al. [54] as well as some metal oxide doped glasses by Aygun et al. [55].

The μ values have been calculated for all the CRT samples and displayed in Fig. 9. Based on this figure, at first (up to about 400 keV), the μ minimizes exponentially over the low energies while the reduction in μ values is linear with increasing of energy (E > 400 keV). This behavior is due to the photoelectric absorption (PE) and Compton scattering (CS) mechanisms which are interaction modes of photon with matter. The photoelectric absorption and Compton scattering are generally more effective mechanisms at E < 400 keV and 400 keV < E < 1332.5 keV, respectively due to that cross sections of these modes are related to the energy as $E^{-3.5}$ and E^{-1} and atomic number as Z^{4-5} and Z, respectively.

The numerical HVL, TVL and MFP values against photon energies have also been represented. Fig. 10a–c is quite enlightening in terms of comparing the attenuation effectiveness of the CRT glasses containing several proportions of Er_2O_3 content. All HVL, TVL and MFP values increase with photon energies and reduce by the increase of Er_2O_3 dopant amount namely WPG5<WPG3<WPG1<WPG0. It means that the insertion of Er_2O_3 chemical to CRT glass implies better shielding material in terms of thickness requirements. The comparison of the HVL values of different studies with that of WPG samples plays a significant role. Fig. 11 demonstrates the comparison of HVLs of WPG glasses systems with ordinary, hematite-serpentine, ilmenite-limonite, steel-scrap and steel-magnetite concretes [56]. It is clear that in the energy region of 276.4–1332.5 keV, Er_2O_3 based WPG glasses are lower HVL than ordinary, hematite-serpentine and ilmenite-limonite concretes whereas higher HVL than those of steel-scrap and steel-magnetite concretes.

The Z_{eff} and N_E values refer to the probabilities of high energetic photon interactions with any absorber. The obtained results for various

Table 5
G-P energy absorption and exposure build-up factor parameters of the WPG1 in the energy range from 0.015 to 15 MeV.

Energy (MeV)	EABF					EBF				
	A	b	c	d	Xk	a	b	c	d	Xk
0.015	0.240	1.017	0.366	−0.139	11.811	0.247	1.018	0.366	−0.166	11.529
0.02	0.279	1.023	0.335	−0.273	19.668	0.274	1.025	0.301	−0.164	14.979
0.03	0.243	1.067	0.353	−0.140	12.623	0.217	1.065	0.382	−0.115	12.296
0.04	0.239	1.082	0.348	−0.128	13.899	0.243	1.082	0.346	−0.125	12.477
0.05	0.235	1.162	0.363	−0.134	14.324	0.224	1.152	0.382	−0.128	14.065
0.06	0.226	1.185	0.379	−0.134	14.706	0.207	1.164	0.409	−0.114	14.177
0.08	0.192	1.338	0.441	−0.109	15.096	0.180	1.265	0.470	−0.098	14.470
0.1	0.167	1.545	0.498	−0.101	16.104	0.149	1.364	0.545	−0.082	14.055
0.15	0.180	2.270	0.528	−0.128	14.246	0.090	1.589	0.709	−0.052	14.055
0.2	0.106	2.700	0.711	−0.086	13.337	0.046	1.744	0.861	−0.035	13.486
0.3	0.034	2.944	0.940	−0.047	12.746	0.003	1.883	1.035	−0.019	12.403
0.4	0.001	2.797	1.075	−0.032	12.161	−0.019	1.913	1.138	−0.014	11.418
0.5	−0.020	2.612	1.157	−0.019	11.568	−0.029	1.909	1.188	−0.011	9.935
0.6	−0.027	2.482	1.186	−0.015	10.786	−0.034	1.888	1.213	−0.009	8.612
0.8	−0.031	2.276	1.203	−0.014	8.925	−0.036	1.846	1.222	−0.012	7.223
1	−0.034	2.136	1.204	−0.010	7.330	−0.033	1.815	1.201	−0.011	7.655
1.5	−0.040	1.938	1.196	0.010	15.373	−0.040	1.754	1.198	0.011	15.888
2	−0.029	1.834	1.145	0.007	17.053	−0.030	1.738	1.147	0.008	17.359
3	−0.008	1.692	1.054	−0.005	12.639	−0.007	1.658	1.054	−0.008	11.249
4	0.010	1.591	0.992	−0.016	12.848	0.009	1.583	1.000	−0.016	10.552
5	0.018	1.509	0.965	−0.026	14.982	0.014	1.514	0.979	−0.018	12.639
6	0.023	1.442	0.951	−0.030	14.624	0.020	1.466	0.959	−0.023	13.521
8	0.030	1.349	0.930	−0.027	12.953	0.031	1.387	0.929	−0.032	13.423
10	0.039	1.290	0.908	−0.038	13.493	0.036	1.324	0.919	−0.035	13.681
15	0.037	1.189	0.925	−0.039	14.270	0.051	1.230	0.892	−0.050	13.306

Er-added CRT glass systems against photon energies of 276.4–1332.5 keV were given in Fig. 12 and Table 3. It is obvious that the Z_{eff} and N_E values vary in the descending order of WPG5>WPG3>WPG1>WPG0. Thus, WPG5 sample among the studied CRT glasses possesses the largest Z_{eff} value at detected gamma ray energies. Its large Z_{eff} can be attributed to its large amount (5%) of Er_2O_3 content and also, the larger interaction of photon with WPG5 glass as compared to rest glasses. The photons rapidly lose energies with this interaction and decrease the penetrating of the photons across WPG5. Additionally, the N_E against photon energy has quite similar trend to that of Z_{eff} owing to direct proportional to the average atomic weight. Lastly, both Z_{eff} and N_E of all Er-doped CRT glasses reduce with the increasing of the gamma rays photon energies as viewed in Fig. 12. The similar change in Z_{eff} is attributed to the replacement of Er content in xEr_2O_3:20ZnO:(80-x)TeO_2 by Tekin et al. [57] and in B_2O_3–TeO_2–PbO–ZnO–Li_2O–Na_2O–Er_2O_3 Lakshmınarayana et al. [51] reported similar results obtained by MCNP method.

3.3. Build up factors and kerma relative to air

Theoretical equivalent atomic numbers for WPG glass series in the energy region 0.015 MeV ≤ E ≤ 15 MeV were listed in Table 4. Also, G-P energy absorption and exposure build-up coefficients in the studied energy range for WPG1 were summarized in Table 5. EABF values of the glass series are shown in Fig. 13 as a function of the incident photon energy in the range from 0.015 MeV to 15 MeV at 0.5, 1, 5, 10, 20 and 40 *mfp*. Fig. 14 showed the EBF values of WPG0, WPG1, WPG3 and WPG5 according to the incident photon energy in the energy region 0.015 MeV ≤ E ≤ 15 MeV for different penetration depths just like Fig. 13. As seen from Figs. 13 and 14, EABF and EBF values of the glass systems demonstrate different characteristics at different energy regions. Energy absorption build-up factor and exposure build-up factor values take minimums and maximums around the low and intermediate energy region, respectively. It is clearly seen from Figs. 13 and 14, photoelectric absorption (PA), Compton scattering (CS) and pair production (PP) photon interaction mechanisms dominate in the low, intermediate and high energy regions, respectively. Also, build-up factors increased with increasing penetration depths. As an example, EABF values for WPG0 take 1.136, 1.219, 1.491, 1.650, 1.879 and 2.091 at 0.5, 1, 5, 10, 20 and 40 *mfp*, respectively. As seen from Fig. 13, EABF values at 40 mfp take maximum at 0.5 MeV for investigated glass series. It is obviously seen from Fig. 14, EBF values at 40 *mfp* show peaks at 0.5 MeV for WPG0 (149.629), at 0.6 MeV for WPG1 (135.943), WPG3 (118.693) and WPG5 (104.613). WPG5 generally received the lowest EABF and EBF values at the low energy region and intermediate energy region among the glass systems. This means that WPG5 is a better radiation absorber than WPG0, WPG1 and WPG3. Also, we can say that EABF and EBF values are dependent on the chemical composition of the glass systems and photon energy.

EABF and EBF values of the glass systems are plotted in Figs. 15 and 16 against the penetration depth at 0.015, 0.15, 1.5 and 15 MeV photon energies. As seen from Figs. 15 and 16, EABF and EBF values for each glass system were generally increased with increasing penetration depth. WPG5 generally received the lowest EABF and EBF values at 0.015 MeV, 0.15 MeV and 1.5 MeV among the glass systems but build-up factors of the WPG5 indicated opposite trend at the 15 MeV and took the highest EABF and EBF values at specially penetration depth 10 *mfp* ≤ PD ≤ 40 *mfp*. This situation can be explained that PP process is more dominant in the high energy region and approximately dependent on Z^2.

Kerma relative to air values of a glass system were calculated from Eq. (7) using the mass energy absorption coefficients taken from Ref. [58]. Kerma relative to air values of the WPG0, WPG1, WPG3 and WPG5 were plotted as a function of energy at the energy region 0.001 MeV ≤ E ≤ 20 MeV in Fig. 17. As seen from Fig. 17, WPG5 generally received the highest kerma relative to air among the glass systems. The contribution of the elements in the glass systems is clearly seen from Fig. 17. It is clearly seen from Fig. 17, Kerma relative to air values sharply increase with increasing the photon energy around the K edge energies of the elements in the WPG0, WPG1, WPG3 and WPG5. Also, contribution of the Erbium in the glass systems is clearly seen at the K shell edge energy of Er (~0.057 MeV). Kerma relative to air values take 21.21 for WPG0, 22.26 for WPG1, 24.29 for WPG3 and 26.38 for WPG5 at ~0.057 MeV (K shell edge energy of Er). As a result, we can say that kerma relative to air values of the WPG0, WPG1, WPG3 and WPG5 are depend on the chemical composition of the glass systems and photon energy just like EABF and EBF.

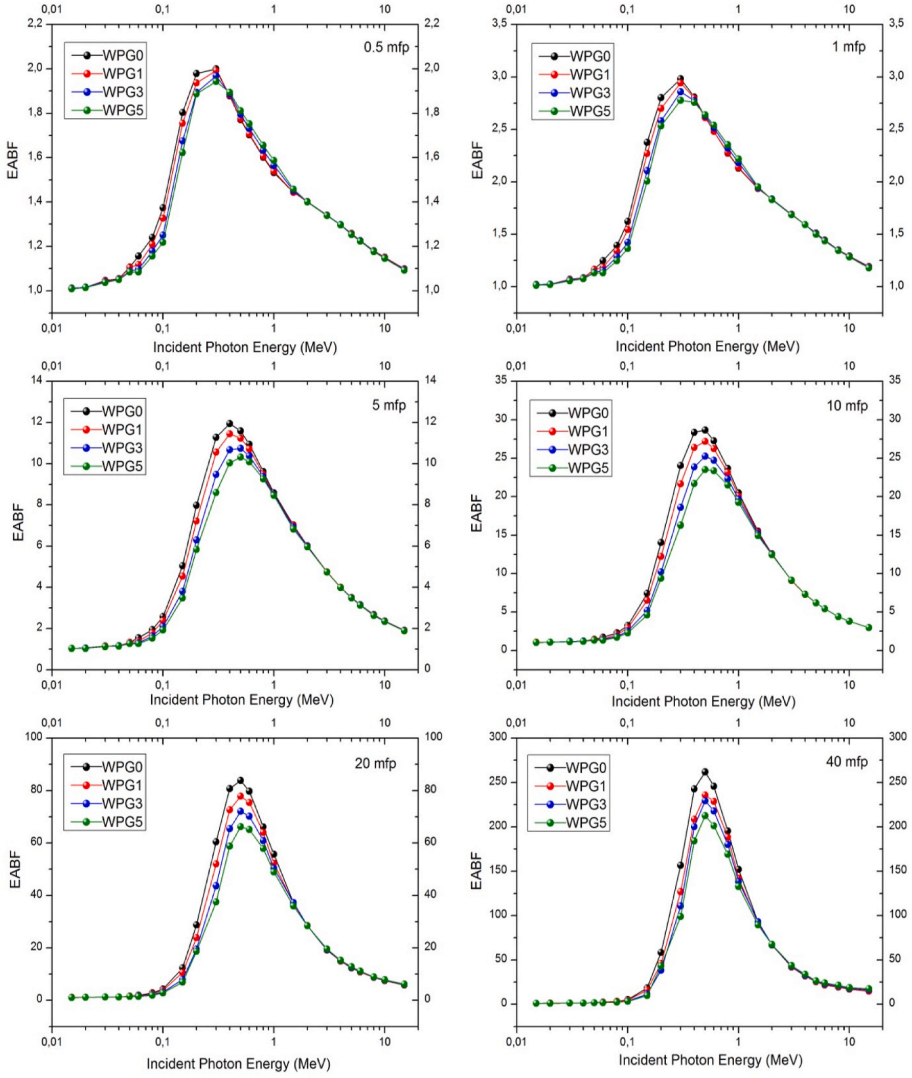

Fig. 13. EABF values of WPG glass series in the energy region 0.015–15 MeV at 0.5, 1, 5, 10, 20 and 40 *mfp*.

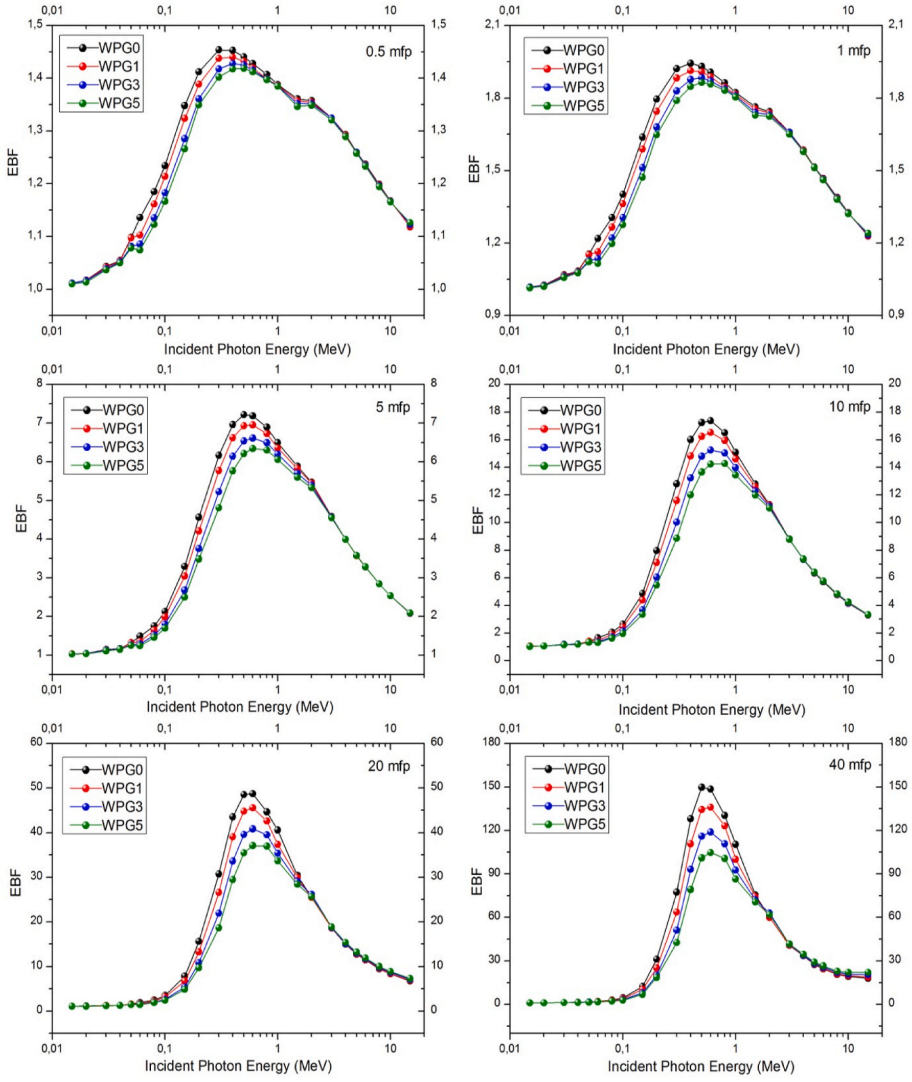

Fig. 14. EBF values of WPG glass series in the energy region 0.015–15 MeV at 0.5, 1, 5, 10, 20 and 40 *mfp*.

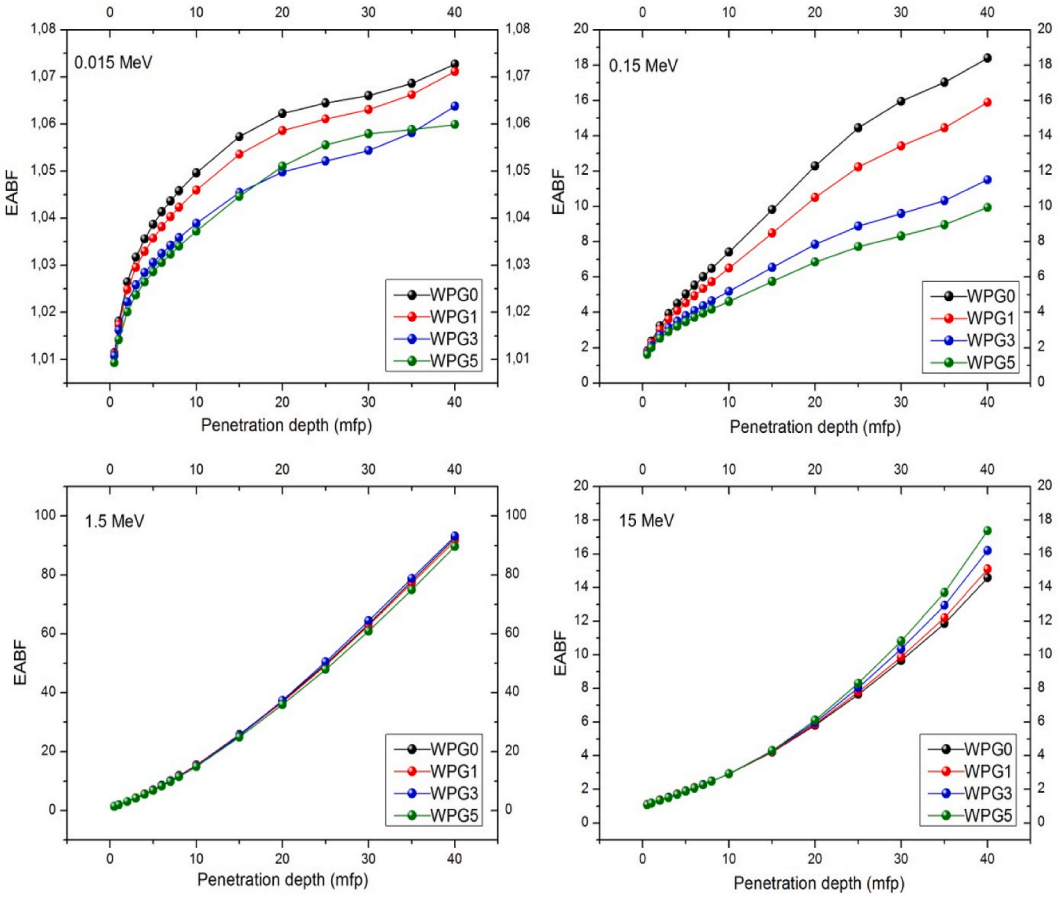

Fig. 15. EABF values of WPG glass series up to 40 *mfp* at 0.015, 0.15, 1.5, 15 MeV.

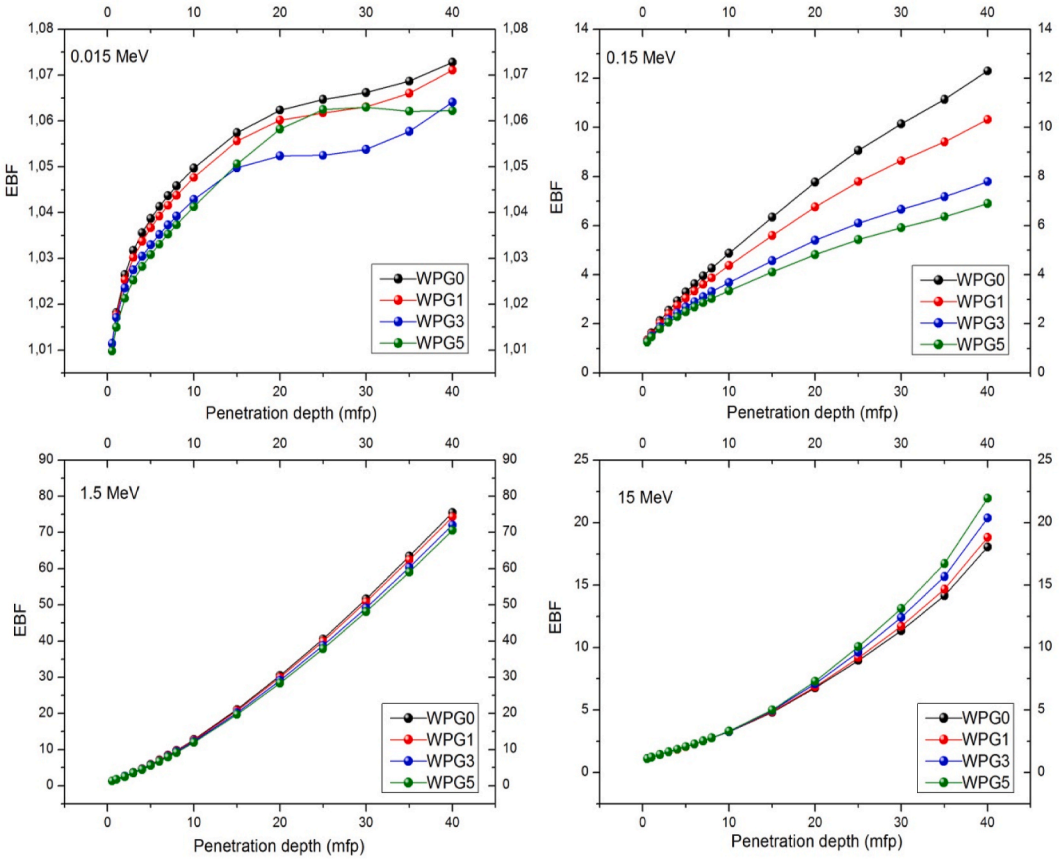

Fig. 16. EBF values of WPG glass series up to 40 *mfp* at 0.015, 0.15, 1.5, 15 MeV.

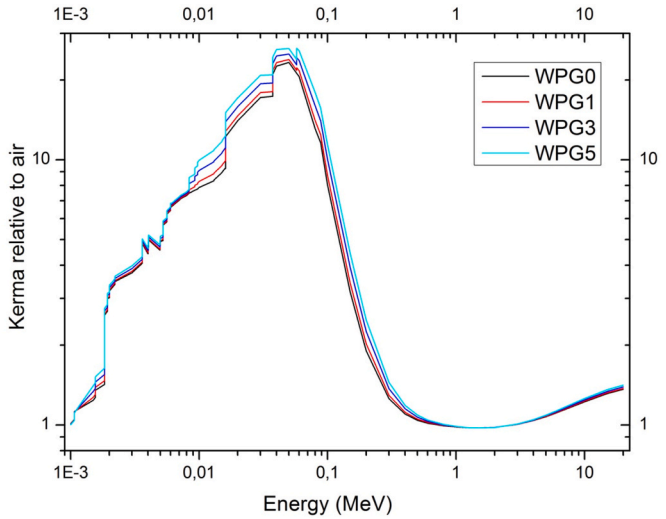

Fig. 17. Kerma relative to air values of WPG glass series in the energy region 0.001–20 MeV.

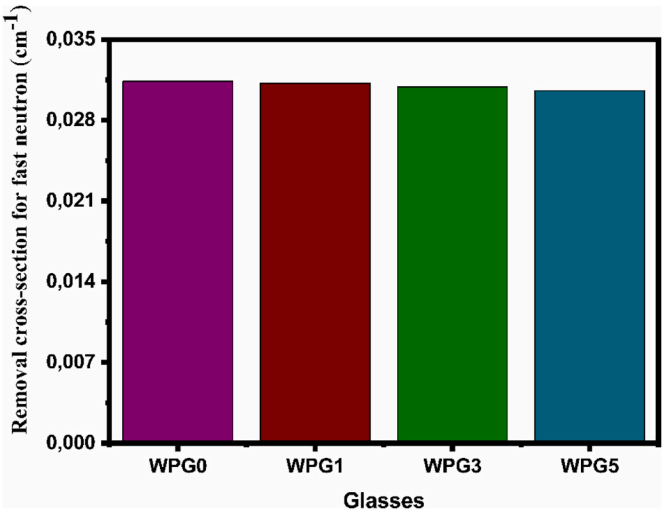

Fig. 18. Fast neutron removal cross sections of the studied CRT glasses.

3.4. Fast neutron removal cross section

The possibility of a neutron particle undergoing certain reaction per unit length when passing through the shield absorber describes the macroscopic effective removal cross sections for fast neutrons Σ_R (cm^{-1}). Therefore, it is related to the elemental composition and partial density values. The estimated Σ_R results of using chemical compositions (Table 1) are displayed in Fig. 18. Based on this figure; it is seeming that as the shielding of CRT glasses for fast neutrons are in descending order of WPG0 (0.0314 cm^{-1})>WPG1 (0.0312 cm^{-1})>WPG3 (0.0309 cm^{-1})> WPG5 (0.0306 cm^{-1}). Since the mass removal cross sections of elements with reducing contents, especially O, Si and K with 0.0405, 0.0295 and 0.0247 cm^2/g, are larger than Er, it can be explained to a result of replacement of Er_2O_3 contents by SiO_2 and K_2O in CRT glasses.

4. Conclusion

This study focuses on revealing that nuclear radiation shielding

performances of CRT glasses are strongly dependent on CRT content. The Er_2O_3 doped waste recycled CRT glasses have been successfully fabricated into new radiation shielding glass and tested for alternative utilization. As a result of this detailed research, the drawn conclusions can be briefly summarized:

- The insertion ratio from 0 to 5 mol% in Er_2O_3 increased the glass density from 2.9216 to 2.9763 g/cm^3.
- All fabricated WPG series demonstrated an amorphous nature irrespective of the Er_2O_3 contribution according to the XRD patterns.
- Morphological determinations via SEM technique clearly confirmed the non-crystalinity of the synthesized glass series. Elemental mapping with the use of EDS/SEM technique revealed the existence of each element in the glass system.
- As results of the radiation shielding performance measured with various gamma-ray transmission tests at different energies, the incorporation of Er_2O_3 as dopant are significantly improved photon shielding effectiveness of CRT glasses by 2.68% times compared to the Er-free CRT sample. Additionally, the experimental μ_m values have been confirmed to those of the theoretical calculation.
- In addition, the highest Σ_R value was found for WPG0 encoded CRT glasses among rest of other studied samples, so it is a best absorber for neutron shielding purposes.
- The results of this study showed that unlike waste industrial material, the recycled CRT glasses with the excellent advantage of developing nuclear radiation attenuation performance may be evaluated as an alternative attenuation absorber. The re-use of such glasses with radiation shield is feasible for utilization in different purposes such as storage/transport containers for nuclear power plants, hospitals for oncology, radioactive waste, diagnostic X-ray and CT-scanner rooms, nuclear research laboratories and may save a great amount in terms of various high-density minerals. Lastly, incorporated CRT glasses may immobilize the Pb to some extent.

Declaration of competing interest

The authors declare that they have no known competing financial interests or personal relationships that could have appeared to influence the work reported in this paper.

Acknowledgement

The authors would like to thank Bingöl University, Central Laboratory Application and Research Center due to contributions in SEM and XRD analyses.

References

[1] R. Kurtulus, T. Kavas, I. Akkurt, K. Gunoglu, An experimental study and WinXCom calculations on X-ray photon characteristics of Bi2O3-and Sb2O3-added waste soda-lime-silica glass, Ceram. Int. 46 (13) (2020) 21120–21127.
[2] C.H. Huang, S.K. Lin, C.S. Chang, H.J. Chen, Mix proportions and mechanical properties of concrete containing very high-volume of Class F fly ash, Construct. Build. Mater. 46 (2013) 71–78.
[3] M.L. Socolof, J.G. Overly, J.R. Geibig, Environmental life-cycle impacts of CRT and LCD desktop computer displays, J. Clean. Prod. 13 (13–14) (2005) 1281–1294.
[4] T.C. Ling, C.S. Poon, A comparative study on the feasible use of recycled beverage and CRT funnel glass as fine aggregate in cement mortar, J. Clean. Prod. 29 (2012) 46–52.
[5] C. Gable, B. Shireman, Computer and electronics product stewardship: are we ready for the challenge? Environ. Qual. Manag. 11 (1) (2001) 35–45.
[6] Q. Song, Z. Wang, J. Li, X. Zeng, Life cycle assessment of TV sets in China: a case study of the impacts of CRT monitors, Waste Manag. 32 (10) (2012) 1926–1936.
[7] W. Meng, X. Wang, W. Yuan, J. Wang, G. Song, The recycling of leaded glass in cathode ray tube (CRT), Procedia Environmental Sciences 31 (2016) 954–960.
[8] F. Méar, P. Yot, M. Cambon, M. Ribes, The characterization of waste cathode-ray tube glass, Waste Manag. 26 (12) (2006) 1468–1476.
[9] N. Saca, L. Radu, V. Fugaru, M. Gheorghe, I. Petre, Composite materials with primary lead slag content: application in gamma radiation shielding and waste encapsulation fields, J. Clean. Prod. 179 (2018) 255–265.
[10] J.S. Lee, H.M. Yoo, S.W. Park, S.J. Cho, Y.C. Seo, Recycling of cathode ray tube panel glasses as aggregates of concrete blocks and clay bricks, J. Mater. Cycles Waste Manag. 18 (3) (2016) 552–562.
[11] X. Tian, The current situation of lead recycling in scrap CRT and the research of technologies comparisons, in: The Feasible Technical Workshop on the Prevention and Control of Heavy Metal Pollution and the Remediation of Soil and Groundwater, 2015, pp. 24–29. http://www.wanfangdata.com.cn/details/detail.do?_type=conference&id=8769323.
[12] Q. Xu, G. Li, W. He, J. Huang, X. Shi, Cathode ray tube (CRT) recycling: current capabilities in China and research progress, Waste Manag. 32 (8) (2012) 1566–1574.
[13] Y. Qi, X. Xiao, Y. Lu, J. Shu, J. Wang, M. Chen, Cathode ray tubes glass recycling: a review, Sci. Total Environ. 650 (2019) 2842–2849.
[14] P. Sopapan, J. Laopaiboon, O. Jaiboon, C. Yenchai, R. Laopaiboon, Feasibility study of recycled CRT glass on elastic and radiation shielding properties used as x-ray and gamma-ray shielding materials, Prog. Nucl. Energy 119 (2020) 103149.
[15] H.L. Liu, J.J. Shi, H.Q. Qu, D.X. Ding, Feasibility of using recycled CRT funnel glass as partial replacement of high density magnetite sand in radiation shielding concrete, Trans. Nonferrous Metals Soc. China 29 (4) (2019) 831–839.
[16] O. Agar, E. Kavaz, E.E. Altunsoy, O. Kilicoglu, H.O. Tekin, M.I. Sayyed, T. T. Erguzel, N. Tarhan, Er2O3 effects on photon and neutron shielding properties of TeO2-Li2O-ZnO-Nb2O5 glass system, Results in Physics 13 (2019) 102277.
[17] Y.S. Rammah, K.A. Mahmoud, E. Kavaz, A. Kumar, F.I. El-Agawany, The role of PbO/Bi2O3 insertion on the shielding characteristics of novel borate glasses, Ceram. Int. 46 (15) (2020) 23357–23368.
[18] A.M. Ali, Y.S. Rammah, M.I. Sayyed, H.H. Somaily, H. Algarni, M. Rashad, The impact of lead oxide on the optical and gamma shielding properties of barium borate glasses, Appl. Phys. A 126 (4) (2020) 1–9.
[19] N.S. Prabhu, V. Hegde, A. Wagh, M.I. Sayyed, O. Agar, S.D. Kamath, Physical, structural and optical properties of Sm3+ doped lithium zinc alumino borate glasses, J. Non-Cryst. Solids 515 (2019) 116–124.
[20] Y.S. Rammah, E. Kavaz, H. Akyildirim, F.I. El-Agawany, Evaluation of photon, neutron, and charged particle shielding competences of TeO2-B2O3-Bi2O3-TiO2 glasses, J. Non-Cryst. Solids 535 (2020) 119960.
[21] F.I. El-Agawany, O.L. Tashlykov, K.A. Mahmoud, Y.S. Rammah, The radiation-shielding properties of ternary SiO2–SnO–SnF2 glasses: simulation and theoretical study, Ceram. Int. 46 (15) (2020) 23369–23378.
[22] U. Perişanoğlu, F.I. El-Agawany, E. Kavaz, M. Al-Buriahi, Y.S. Rammah, Surveying of Na2O3–BaO–PbO–Nb2O5–SiO2–Al2O3 glass-ceramics system in terms of alpha, proton, neutron and gamma protection features by utilizing GEANT4 simulation codes, Ceram. Int. 46 (3) (2020) 3190–3202.
[23] H.O. Tekin, E. Kavaz, E.E. Altunsoy, M. Kamislioglu, O. Kilicoglu, O. Agar, M. I. Sayyed, N. Tarhan, Characterization of a broad range gamma-ray and neutron shielding properties of MgO-Al2O3-SiO2-B2O3 and Na2O-Al2O3-SiO2 glass systems, J. Non-Cryst. Solids 518 (2019) 92–102.
[24] F.I. El-Agawany, K.A. Mahmoud, E. Kavaz, R. El-Mallawany, Y.S. Rammah, Evaluation of nuclear radiation shielding competence for ternary Ge–Sb–S chalcogenide glasses, Appl. Phys. A 126 (4) (2020) 1–11.
[25] M.I. Sayyed, K.M. Kaky, E. Şakar, U. Akbaba, M.M. Taki, O. Agar, Gamma radiation shielding investigations for selected germanate glasses, J. Non-Cryst. Solids 512 (2019) 33–40.
[26] Y.S. Rammah, G. Kilic, R. El-Mallawany, U.G. Issever, F.I. El-Agawany, Investigation of optical, physical, and gamma-ray shielding features of novel vanadyl boro-phosphate glasses, J. Non-Cryst. Solids 533 (2020) 119905.
[27] Y.S. Rammah, K.A. Mahmoud, M.I. Sayyed, F.I. El-Agawany, R. El-Mallawany, Novel vanadyl lead-phosphate glasses: P2O5–PbO–ZnONa2O–V2O5: synthesis, optical, physical and gamma photon attenuation properties, J. Non-Cryst. Solids 534 (2020) 119944.
[28] O. Agar, M.I. Sayyed, H.O. Tekin, K.M. Kaky, S.O. Baki, I. Kityk, An investigation on shielding properties of BaO, MoO3 and P2O5 based glasses using MCNPX code, Results in Physics 12 (2019) 629–634.
[29] Y.S. Rammah, Evaluation of radiation shielding ability of boro-tellurite glasses: TeO 2–B 2 O 3–SrCl 2–LiF–Bi 2 O 3, Appl. Phys. A 125 (12) (2019) 1–11.
[30] M.S. Al-Buriahi, F.I. El-Agawany, C. Sriwunkum, H. Akyıldırım, H. Arslan, B. T. Tonguc, R. El-Mallawany, Y.S. Rammah, Influence of Bi2O3/PbO on nuclear shielding characteristics of lead-zinc-tellurite glasses, Phys. B Condens. Matter 581 (2020) 411946.
[31] Y. Al-Hadeethi, M.I. Sayyed, O. Agar, Ionizing photons attenuation characterization of quaternary tellurite–zinc–niobium–gadolinium glasses using Phy-X/PSD software, J. Non-Cryst. Solids 538 (2020) 120044.
[32] R. Laopaiboon, C. Bootjomchai, M. Chanphet, J. Laopaiboon, Elastic properties investigation of gamma-radiated barium lead borosilicate glass using ultrasonic technique, Ann. Nucl. Energy 38 (11) (2011) 2333–2337.
[33] H. Zhao, C.S. Poon, T.C. Ling, Utilizing recycled cathode ray tube funnel glass sand as river sand replacement in the high-density concrete, J. Clean. Prod. 51 (2013) 184–190.
[34] P. Walczak, J. Małolepszy, M. Reben, K. Rzepa, Mechanical properties of concrete mortar based on mixture of CRT glass cullet and fluidized fly ash, Procedia Engineering 108 (2015) 453–458.
[35] F. Akman, I. Ozkan, M.R. Kaçal, H. Polat, S.A. Issa, H.O. Tekin, O. Agar, Shielding features, to non-ionizing and ionizing photons, of FeCr-based composites, Appl. Radiat. Isot. 167 (2020) 109470.
[36] P. Limkitjaroenporn, J. Kaewkhao, P. Limsuwan, W. Chewpraditkul, Physical, optical, structural and gamma-ray shielding properties of lead sodium borate glasses, J. Phys. Chem. Solid. 72 (4) (2011) 245–251.

[37] H.O. Tekin, E. Kavaz, E.E. Altunsoy, O. Kilicoglu, O. Agar, T.T. Erguzel, M. I. Sayyed, An extensive investigation on gamma-ray and neutron attenuation parameters of cobalt oxide and nickel oxide substituted bioactive glasses, Ceram. Int. 45 (8) (2019) 9934–9949.
[38] A. Sharma, M.I. Sayyed, O. Agar, M.R. Kaçal, H. Polat, F. Akman, Photon-shielding performance of bismuth oxychloride-filled polyester concretes, Mater. Chem. Phys. 241 (2020) 122330.
[39] M.R. Kacal, H. Polat, M. Oltulu, F. Akman, O. Agar, H.O. Tekin, Gamma shielding and compressive strength analyses of polyester composites reinforced with zinc: an experiment, theoretical, and simulation based study, Appl. Phys. A 126 (3) (2020) 1–15.
[40] N.S. Prabhu, V. Hegde, A. Wagh, M.I. Sayyed, O. Agar, S.D. Kamath, Physical, structural and optical properties of Sm3+ doped lithium zinc alumino borate glasses, J. Non-Cryst. Solids 515 (2019) 116–124.
[41] M.R. Kaçal, K. Dilsiz, F. Akman, H. Polat, Analysis of radiation attenuation properties for polyester/Li2WO4 composites, Radiat. Phys. Chem. (2020), 109257.
[42] M.F. Turhan, F. Akman, H. Polat, M.R. Kaçal, İ. Demirkol, Gamma-ray attenuation behaviors of hematite doped polymer composites, Prog. Nucl. Energy 129 (2020) 103504.
[43] NNDC, 2020. http://www.nndc.bnl.gov/nudat2/reCenter.jsp?Z=28 & n=32 (Accesed [25.11].20)..
[44] M.R. Kacal, F. Akman, M.I. Sayyed, Investigation of radiation shielding properties for some ceramics, Radiochim. Acta 107 (2) (2019) 179–191.
[45] M.I. Sayyed, H.O. Tekin, O. Agar, Gamma photon and neutron attenuation properties of MgO–BaO–B2O3–TeO2–Cr2O3 glasses: the role of TeO2, Radiat. Phys. Chem. 163 (2019) 58–66.
[46] F.H. Attix, Introduction to Radiological Physics and Radiation Dosimetry, WILEY-VCH Verlag GmbH & Co. KGaA, 1986 (Chapter 2), Page 22.
[47] O. Kilicoglu, E.E. Altunsoy, O. Agar, M. Kamislioglu, M.I. Sayyed, H.O. Tekin, N. Tarhan, Synergistic effect of La2O3 on mass stopping power (MSP)/projected range (PR) and nuclear radiation shielding abilities of silicate glasses, Results in Physics 14 (2019) 102424.
[48] N.S. Prabhu, K. Sharmila, H.M. Somashekarappa, G. Lakshminarayana, S. Mandal, M.I. Sayyed, S.D. Kamath, Thermoluminescence features of Er3+ doped BaO-ZnO-LiF-B2O3 glass system for high-dose gamma dosimetry, Ceram. Int. 46 (11) (2020) 19343–19353.
[49] S. Yalcin, B. Aktas, D. Yilmaz, Radiation shielding properties of Cerium oxide and Erbium oxide doped obsidian glass, Radiat. Phys. Chem. 160 (2019) 83–88.
[50] S.A. Tijani, S.M. Kamal, Y. Al-Hadeethi, M. Arib, M.A. Hussein, S. Wageh, L.A. Dim, Radiation shielding properties of transparent erbium zinc tellurite glass system determined at medical diagnostic energies, J. Alloys Compd. 741 (2018) 293–299.
[51] G. Lakshminarayana, M.I. Sayyed, S.O. Baki, A. Lira, M.G. Dong, K.A. Bashar, I. V. Kityk, M.A. Mahdi, Borotellurite glasses for gamma-ray shielding: an exploration of photon attenuation coefficients and structural and thermal properties, J. Electron. Mater. 48 (2) (2019) 930–941.
[52] O. Agar, M.I. Sayyed, F. Akman, H.O. Tekin, M.R. Kaçal, An extensive investigation on gamma ray shielding features of Pd/Ag-based alloys, Nuclear Engineering and Technology 51 (3) (2019) 853–859.
[53] Y.S. Rammah, M.S. Al-Buriahi, A.S. Abouhaswa, B2O3–BaCO3–Li2O3 glass system doped with Co3O4: structure, optical, and radiation shielding properties, Phys. B Condens. Matter 576 (2020) 411717.
[54] A. Kumar, D.K. Gaikwad, S.S. Obaid, H.O. Tekin, O. Agar, M.I. Sayyed, Experimental studies and Monte Carlo simulations on gamma ray shielding competence of (30+ x) PbO10WO3 10Na2O− 10MgO–(40-x) B2O3 glasses, Prog. Nucl. Energy 119 (2020) 103047.
[55] B. Aygün, E. Şakar, E. Cinan, N.Y. Yorgun, M.I. Sayyed, O. Agar, A. Karabulut, Development and production of metal oxide doped glasses for gamma ray and fast neutron shielding, Radiat. Phys. Chem. 174 (2020) 108897.
[56] I.I. Bashter, Calculation of radiation attenuation coefficients for shielding concretes, Ann. Nucl. Energy 24 (17) (1997) 1389–1401.
[57] H.O. Tekin, V.P. Singh, E.E. Altunsoy, M. Karahan, M.I. Sayyed, T.T. Erguzel, E. S. Kasikci, M. Konuk, Gamma shielding properties of erbium zinc tellurite glass system using Monte Carlo method, J. Test. Eval. 48 (2) (2020) 1252–1261.
[58] J.H. Hubbell, S.M. Seltzer, *Tables Of X-Ray Mass Attenuation Coefficients and Mass Energy-Absorption Coefficients 1 keV to 20 MeV for Elements Z= 1 to 92 and 48 Additional Substances of Dosimetric Interest* (No. PB-95-220539/XAB; NISTIR-5632). National Inst. Of Standards and Technology-PL, Ionizing Radiation Div, Gaithersburg, MD (United States), 1995.